Bistatic Synthetic Aperture Radar Imaging for Arbitrary Flight Trajectories and Non-flat Topography

Can Evren Yarman and Birsen Yazıcı
Department of Electrical, Computer
and System Engineering
Rensselaer Polytechnic Institute
Troy, New York 12180–3590
Email: yarman,yazici@ecse.rpi.edu

Margaret Cheney
Department of Mathematical Sciences
Rensselaer Polytechnic Institute
Troy, New York 12180
Email: cheney@rpi.edu

Abstract— **This paper presents an approximate analytic inversion method for bistatic synthetic aperture radar. A scene of interest is illuminated by electromagnetic waves that are transmitted from positions along an arbitrary, but known, flight trajectory and the scattered waves are measured from positions along a different flight trajectory which is also arbitrary, but known. We assume a single-scattering model for the radar data, and we assume that the ground topography is known but not necessarily flat. We use microlocal analysis to develop a filtered-backprojection-type reconstruction method.**

I. Introduction

In synthetic aperture radar (SAR) imaging a scene of interest is illuminated by electromagnetic waves that are transmitted from an antenna mounted on a plane or satellite. The aim is to reconstruct an image of the scene from the measurement of the scattered waves.

In bistatic SAR [1], unlike the monostatic case, where transmitter and receiver antennas are co-located, (Figure 1.a), transmitter and receiver antennas are located on separate platforms (Figure 1.b). This allows the transmitter and its heavy power supply to be flown on a platform different from that of the cheap, expendable receiver. Also, some of the electronic countermeasures that have been devised to thwart monostatic configurations are less effective against bistatic systems [2], [3], [1]. Finally, bistatic measurements can provide better ability to distinguish targets from clutter [4].

For SAR systems whose antennas are able to form a narrow beam, the image reconstruction algorithms are well-known [5], [6], [7], [8], [9], [10], [11]. However these algorithms are not useful for imaging systems using antennas having poor directivity where the antenna footprint is large.

In [12], [13], [14], [15], [16], reconstruction algorithms for monostatic SAR with poor antenna directivity traversing straight and arbitrary flight trajectories have been developed. To our knowledge, the acquisition geometry of bistatic SAR studies for the case of poor antenna directivity are limited to isotropic antennas traversing certain flight trajectories (straight [17], [18] or circular [19], [20] flight trajectories) over flat topography. In this paper, we focus on bistatic SAR with poor antenna directivity and address the image reconstruction problem when transmitter and receiver are traversing arbitrary, but known, flight trajectories over a known, but not necessarily flat, topography.

In particular, we have used microlocal techniques to develop an approximate analytic image reconstruction method for bistatic SAR. Microlocal techniques give rise to a filtered-backprojection-type (FBP) reconstruction method, which, if an exact inversion is possible, often reduces to the exact inversion formula.

The organization of the paper is as follows. In Section II, we introduce our forward model. In Section III, we develop filtered backprojection type image formation process. Finally, Section IV we present numerical simulations to illustrate our

1-4244-0284-0/07/$20.00 ©2007 IEEE

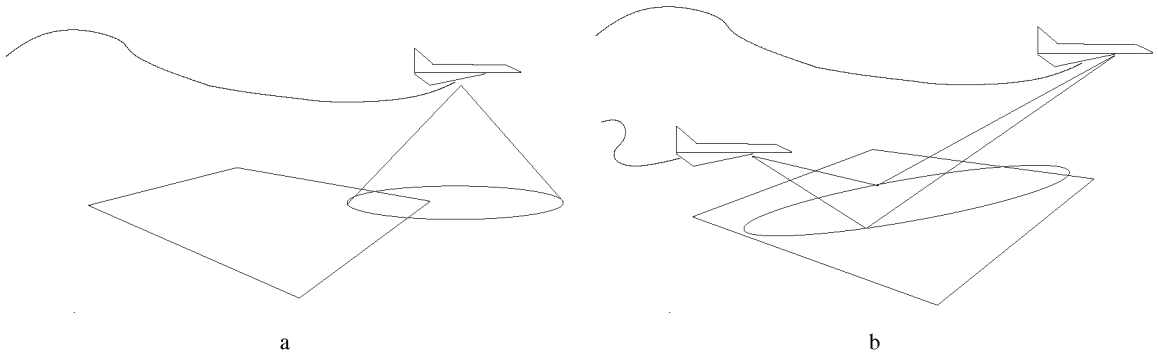

a b

Fig. 1. Acquisition geometry for (left) monostatic and (right) bistatic SAR.

theoretical results. We conclude our discussion with Section V.

II. Forward Model

Let $\boldsymbol{\gamma}_T(s), \boldsymbol{\gamma}_R(s) \in \mathbb{R}^3$, $s \in \mathbb{R}$, be the transmitter and receiver trajectories, respectively. We assume that the earth's surface is located at the position $\mathbf{x} = (x_1, x_2, \psi(x_1, x_2))$, where $\psi : \mathbb{R}^2 \to \mathbb{R}$, is a known smooth function, and scattering takes place in a thin region near the surface. Following [13], [14], under the single scattering (Born) approximation, we model the received signal $d(s,t)$ as follows:

$$d(s,t) \approx \mathcal{F}[V](s,t) := \int \mathrm{e}^{-\mathrm{i}2\pi\omega(t-R_{TR}(s,\boldsymbol{x}))/c_0} \times A_{TR}(\boldsymbol{x}, s, \omega) V(\boldsymbol{x}) d\omega \, d\boldsymbol{x}, \quad (1)$$

where $\boldsymbol{x} = (x_1, x_2)$, $R_{TR}(s, \mathbf{x}) = |\boldsymbol{\gamma}_T(s) - \mathbf{x}| + |\mathbf{x} - \boldsymbol{\gamma}_R(s)|$ is the total travel time, $T(\boldsymbol{x})$ denotes the surface reflectivity, c_0 denotes the speed of light, and A_{TR} is a complex amplitude function that includes the transmitter and receiver antenna beam patterns, the transmitted waveform, geometrical spreading factors, etc. Here t denotes the (fast) time and s, which is referred to as the slow time, parameterizes the trajectory.

Unless otherwise stated, the bold Roman, bold italic, and Roman small letters will denote points in $\mathbb{R}^3$, $\mathbb{R}^2$ and $\mathbb{R}$, respectively, i.e. $\mathbf{x} = (\boldsymbol{x}, x_3) \in \mathbb{R}^3$, with $\boldsymbol{x} \in \mathbb{R}^2$, and $x_3 \in \mathbb{R}$.

We assume that for some m_A, A satisfies the symbol estimate[13], [14]

$$\sup_{(s,\boldsymbol{x})\in K} |\partial_\omega^\alpha \partial_s^\beta \partial_{x_1}^{\rho_1} \partial_{x_2}^{\rho_2} A(\boldsymbol{x}, s, \omega)| \leq C_0 \, (1+\omega^2)^{(m_A - |\alpha|)/2} \quad (2)$$

where K is any compact subset of $\mathbb{R} \times \mathbb{R}^2$, and the constant C_0 depends on K, α, β, ρ_1, and ρ_2. This assumption is needed in order to make various stationary phase calculations hold; in fact this assumption makes the "forward" operator $\mathcal{F}$ is a *Fourier Integral Operator* [21], [22], [23].

The ideal image formation problem is to estimate T from knowledge of $d(s,t)$ for some range of s and t.

III. Image Formation

In general, the strategy for estimating T is to apply an imaging operator $\mathcal{K}$ to the data $\mathcal{F}[T]$. The image $\tilde{T}$ for the target scene can thus be written $\tilde{T} = \mathcal{K}\mathcal{F}[T]$. The operator $\mathcal{L} = \mathcal{K}\mathcal{F}$ contains the information about how the image $\tilde{T}$ is related to the actual target scene T. The kernel of $\mathcal{L}$ is called the *point spread function*.

Our strategy is to determine $\mathcal{K}$ so that the point spread function of $\mathcal{L}$ approximates the Dirac-delta function. In this regard, we extend the monostatic SAR reconstruction techniques based on microlocal analysis [13], [14] to bistatic SAR to determine $\mathcal{K}$.

The microlocal-analysis-based reconstruction method can be viewed as a generalized filtered-backprojection-type reconstruction method where the data is first filtered and then backprojected. It is a direct consequence of microlocal analysis of the backprojection (BP) operator that the visible edges of the scene appear in the correct location and correct orientation in the image obtained by backprojection [13], [14].

We use the following backprojection operator $\mathcal{K}$

to form an image $\tilde{T}$ of the target scene:

$$\begin{aligned}\tilde{T}(\boldsymbol{z}) &:= \mathcal{K}[d](\boldsymbol{z}) \\ &:= \int \mathrm{e}^{\mathrm{i}2\pi\omega(t-R_{TR}(s,\mathbf{z})/c_0)} Q_{TR}(\boldsymbol{z},s,\omega) d(s,t) d\omega\, ds\, dt\end{aligned} \tag{3}$$

where $\mathbf{z} = (\boldsymbol{z}, \psi(\boldsymbol{z}))$and Q_{TR} is the filter to be determined below.

Substituting (1) into (3) results in

$$\tilde{T} = \mathcal{K}\mathcal{F}[T](\boldsymbol{z}) = \mathcal{L}[T](\boldsymbol{z}) = \int L(\boldsymbol{z},\boldsymbol{x}) T(\boldsymbol{x}) d\boldsymbol{x}, \tag{4}$$

where

$$\begin{aligned}L(\boldsymbol{z},\boldsymbol{x}) = \int \mathrm{e}^{\mathrm{i}2\pi\omega\,[R_{TR}(s,\mathbf{x})-R_{TR}(s,\mathbf{z})]/c_0} Q_{TR}(\boldsymbol{z},s,\omega) \\ \times A_{TR}(\boldsymbol{x},s,\omega) d\omega\, ds\end{aligned} \tag{5}$$

is the point spread function. We would like to make $L(\boldsymbol{z},\boldsymbol{x})$ as close as possible to the Dirac delta function $\delta(\boldsymbol{x}-\boldsymbol{z}) = \int \exp(\mathrm{i}2\pi(\boldsymbol{x}-\boldsymbol{z})\cdot\boldsymbol{\xi})\, d\boldsymbol{\xi}$.

The main contribution to $L(\boldsymbol{z},\boldsymbol{x})$ come from those critical points of its phase at which A_{TR} is non-zero. We will assume that the flight trajectories and antenna beam patterns of the transmitter and receiver are focused on a side of their flight trajectories so that the only critical point is $\boldsymbol{x} = \boldsymbol{z}$.

We write

$$[R_{TR}(s,\mathbf{x}) - R_{TR}(s,\mathbf{z})] = (\boldsymbol{x}-\boldsymbol{z})\cdot\Xi(s,\boldsymbol{x},\boldsymbol{z}). \tag{6}$$

For fixed $\boldsymbol{x}$ and $\boldsymbol{z}$, we make the change of variables

$$(s,\omega) \rightarrow \boldsymbol{\xi} = \frac{\omega}{c_0}\Xi(s,\boldsymbol{x},\boldsymbol{z}), \tag{7}$$

in the integral of (5), and obtain

$$\begin{aligned}L(\boldsymbol{z},\boldsymbol{x}) = \int \mathrm{e}^{\mathrm{i}(\boldsymbol{x}-\boldsymbol{z})\cdot\boldsymbol{\xi}} Q_{TR}(\boldsymbol{z},\boldsymbol{\xi}) \\ \times A_{TR}(\boldsymbol{x},\boldsymbol{\xi})\eta(\boldsymbol{x},\boldsymbol{z},\boldsymbol{\xi}) d\boldsymbol{\xi},\end{aligned} \tag{8}$$

where $Q_{TR}(\boldsymbol{z},\boldsymbol{\xi}) = Q_{TR}(\boldsymbol{z}, s(\boldsymbol{\xi}), \omega(\boldsymbol{\xi}))$, etc. and

$$\eta(\boldsymbol{x},\boldsymbol{z},\boldsymbol{\xi}) = |\partial(s,\omega)/\partial\boldsymbol{\xi}|, \tag{9}$$

is the determinant of the Jacobian that comes from the change of variables (7).

Using the method of stationary phase, under assumption (2), the leading order contribution to $\tilde{T}$ is

$$\begin{aligned}\tilde{T} = \mathcal{L}[T](\boldsymbol{z}) \approx \int \mathrm{e}^{\mathrm{i}(\boldsymbol{x}-\boldsymbol{z})\cdot\boldsymbol{\xi}} Q_{TR}(\boldsymbol{z},\boldsymbol{\xi}) A_{TR}(\boldsymbol{z},\boldsymbol{\xi}) \\ \times \eta(\boldsymbol{z},\boldsymbol{z},\boldsymbol{\xi}) T(\boldsymbol{x}) d\boldsymbol{x} d\boldsymbol{\xi}.\end{aligned} \tag{10}$$

With the choice

$$Q_{TR}(\boldsymbol{z},s,\omega) = \frac{\chi_{\Omega_{\boldsymbol{z}}}(\boldsymbol{\xi}(s,\omega))\ \overline{A_{TR}(\boldsymbol{z},s,\omega)}}{\eta(\boldsymbol{z},\boldsymbol{z},\boldsymbol{\xi})\ |A_{TR}(\boldsymbol{z},s,\omega)|^2}, \tag{11}$$

where $\Omega_z = \{\boldsymbol{\xi} = \omega\Xi(s,\boldsymbol{z},\boldsymbol{z}) \mid A_{TR}(\boldsymbol{z},s,\omega) \neq 0\}$ and $\chi_{\Omega_{\boldsymbol{z}}}$ is a smooth cut of function equal to one in the interior of Ω_z and zero in the exterior of Ω_z, (10) becomes

$$\tilde{T}(\boldsymbol{z}) = \mathcal{K}\mathcal{F}[T](\boldsymbol{z}) \approx \int_{\Omega_z} \mathrm{e}^{\mathrm{i}(\boldsymbol{x}-\boldsymbol{z})\boldsymbol{\xi}} \chi_{\Omega_{\boldsymbol{z}}}(\boldsymbol{\xi}) T(\boldsymbol{x}) d\boldsymbol{x} d\boldsymbol{\xi}. \tag{12}$$

Equation (12) shows that the image $\tilde{T}$ is a band-limited version of T whose frequency content, using (7), is determined by the union of $\Omega_{\boldsymbol{z}}$. Mircolocal analysis of (12) tells us that an edge E passing through the point $\boldsymbol{z}$ is visible if the direction $\boldsymbol{n_z}$ normal to the edge is contained in Ω_z [24], [13], [14]. Thus by (12) one can only reconstruct the visible edges of T, in the aforementioned sense.

The $\overline{A_{TR}}/|A_{TR}|^2$ part of the filter corresponds to composition of operations such as matched filtering, beam forming, compensation of geometrical spreading factors, etc. In this regard, the proposed method is a generalization of previously presented reconstruction methods [18], [17], [19], [20].

IV. Numerical Simulations

In our numerical simulations, we considered a square target of size $5.5\mathrm{km}$ located at the center of the scene of size $[0,22]\times[0,22]\,\mathrm{km}^2$ (Figure 2) which is discretized by 128×128 pixels, and a circular flight trajectory $\boldsymbol{\gamma}(s) = (11+22\cos s, 11+22\sin s, 6.5)\,\mathrm{km}$, uniformly sampled for $s\in[0,2\pi)$ at 256 points.

We performed three numerical experiments: Monostatic SAR, bistatic SAR with circular trajectories, and bistatic SAR with fixed transmitter. For comparison reasons, we also implemented backprojection operation [17], [20], where we set $Q=1$.

For monostatic SAR, we set $\gamma_T(s) = \gamma_R(s) = \gamma(s)$. The projection data and reconstructed images are presented in Figure 3. For bistatic SAR, we set the transmitter and the receiver trajectories to be $\gamma_T(s) = \gamma(s)$ and $\gamma_R(s) = \gamma(s+\pi/4)$, respectively. The projection data and reconstructed images are presented in Figure 4. Finally, for bistatic SAR with fixed transmitter, we set the transmitter location to be $\gamma_T = (0, 0, 6.5)$ km and choose the receiver trajectory to be $\gamma_R(s) = \gamma(s)$.

Since we chose a circular trajectory, for any z all the directions in $\mathbb{R}^2$ are contained in Ω_z. Thus all the edges off the target should be visible. This is confirmed by our numerical simulations. Both backprojection and filtered-backprojection preserves the edges in the reconstructed images.

V. Conclusion

In this paper, we developed a new explicit filtered-backprojection type bistatic SAR inversion method for arbitrary flight trajectories. The method is based on microlocal analysis and preserves the location and orientation of the visible edges.

We demonstrate the performance of the proposed algorithm with numerical simulations, which confirms the properties of the presented method.

Acknowledgments

We are grateful to Air Force Office of Scientific Research[1] for supporting this work under the agreements FA9550-04-1-0223 and FA9550-06-1-0017.

References

[1] N. J. Willis, *Bistatic Radar*. Norwood, MA: Artech House, 1991.

[2] W. Goj, *Synthetic Aperture Radar and Electronic Warfare*. Boston: Artech House, 1989.

[3] A. Horne and G. Yates, "Bistatic synthetic aperture radar," in *IEEE RADAR 2002*, Oct. 2002, pp. 6 – 10.

[4] L. Ulander and T. Martin, "Bistatic ultrawideband sar for imaging of groud targets under foliage," in *Proceedings of 2005 IEEE Radar Conference*, May 2005, pp. 419 – 423.

[5] D. Munson, J. O'Brien, and W. Jenkins, "A tomographic formula of spotlight-mode synthetic aperture radar," in *Proceedings of the IEEE*, vol. 72, Aug. 1983, pp. 917–925.

[6] O. Arikan and D. M. Jr., "A tomographic formulation of bistatic synthetic aperture radar," in *Proceedings of ComCon 88*, Oct. 1988, p. 418.

[7] J. Curlander and R. McDonough, *Synthetic Aperture Radar*. New York: Wiley, 1991.

[8] G. Franceschetti and R. Lanari, *Synthetic Aperture Radar Processing*. New York: CRC Press, 1999.

[9] M. Soumekh, *Synthetic Aperture Radar Signal Processing with MATLAB Algorithms*. New York: Wiley, 1999.

[10] L. Cutrona, *Synthetic Aperture Radar*. New York: McGraw-Hill, 1990.

[11] C. Elachi, *Spaceborne Radar Remote Sensing: Applications and Techniques*. New York: IEEE Press, 1987.

[12] S. Nilsson, "Application of fast backprojection techniques for some inverse problems of integral geometry," Ph.D. dissertation, Linköping Studies in Science and Technology, 1997, dissertation No. 499.

[13] C. J. Nolan and M. Cheney, "Synthetic aperture inversion," *Inverse Problems*, vol. 18, pp. 221–236, 2002.

[14] C. Nolan and M. Cheney, "Synthetic aperture inversion for arbitrary flight paths and non-flat topography," *IEEE Transactions on Image Processing*, vol. 12, pp. 1035–1043, 2003.

[15] L. Ulander, H. Hellsten, and G. Stenström, "Synthetic-aperture radar processing using fast factorized back-projection," *IEEE Transactions on Aerospace and electronic systems*, vol. 39, pp. 760–776, 2003.

[16] B. Yazici and M. Cheney, "Synthetic aperture inversion for arbitrary flight paths in the presence of noise and clutter," in *Proceedings of IEEE International Radar Conference*, May 2005, pp. 806–810.

[17] M. Soumekh, "Wide-bandwidth continuous-wave monostatic/bistatic synthetic aperture radar imaging," in *Proceedings of International Conference on Image Processing*, vol. 3, Oct. 1998, pp. 361–365.

[18] ——, "Bistatic synthetic aperutre radar inversion with application in dynamic object imaging," *IEEE Transactions on Signal Processing*, vol. 39, pp. 2044–2055, Sept. 1991.

[19] J. Bauck and W. Jenkins, "Convolution-backprojection image reconstruction for bistatic synthetic aperture radar," in *Proceedings of IEEE ISCAS*, 1989, pp. 1512–1515.

[20] S. Lockwood, A. Brown, and H. Lee, "Backward propagation image reconstruction techniques for bistaticsynthetic-aperture radar imaging systems with circular-apertureconfigurations," in *Proceedings of the Thirty-Fifth Asilomar Conference on Signals, Systems and Computers*, vol. 1, Nov. 2001, pp. 110–115.

[21] J. J. Duistermaat, *Fourier Integral Operators*. Boston: Birkhauser, 1996.

[22] F. Treves, *Introduction to Pseudodifferential and Fourier Integral Operators, volumes I and II*. NY: Plenum Press, 1980.

[23] A. Grigis and J. Sjöstrand, *Microlocal Analysis for Differential Operators: An Introduction*, ser. London Mathematical Society Lecture Note Series, Vol. 196. Cambridge: Cambridge University Press, 1994.

[24] E. Quinto, "Singularities of the x-ray transform and limited data tomography in r^2 and r^3," *SIAM J. Math. Anal.*, vol. 24, pp. 1215–1225, 1993.

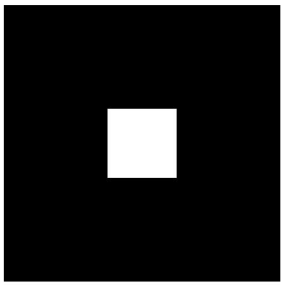

Fig. 2. Scene used in numerical simulations. $(0, 0, 0)$ km and $(22, 22, 0)$ km are located at the lower left and upper right corners, respectively.

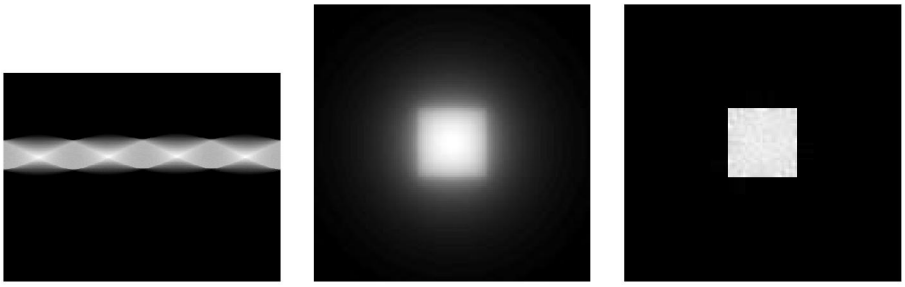

Fig. 3. (Left) Projection data for monostatic SAR and reconstructed images obtained by (middle) backprojection and (right) filtered backprojection.

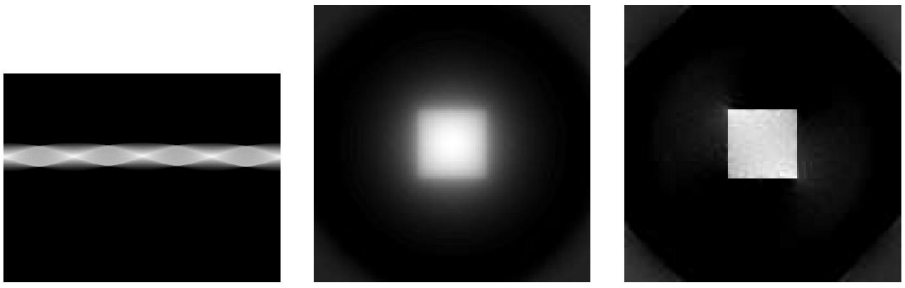

Fig. 4. (Left) Projection data for bistatic SAR for circular transmitter and receiver trajectories and reconstructed images obtained by (middle) backprojection and (right) filtered backprojection.

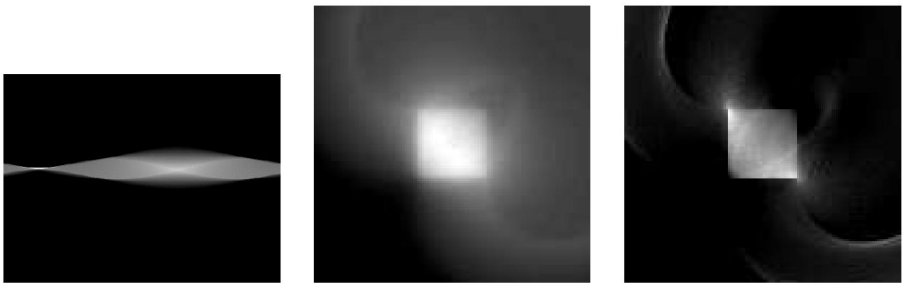

Fig. 5. (Left) Projection data for bistatic SAR with fixed transmitter and reconstructed images obtained by (middle) backprojection and (right) filtered backprojection.